1   Experimental validation of acoustic inversions for high
2   concentration profiling of spherical particles, using broadband
3   technology in the Rayleigh regime

4   Alastair S. Tonge[a,*], Jeffrey Peakall[b], David M.J. Cowell[c], Steven Freear[c], Martyn

5   Barnes[d], Timothy N. Hunter[a,*]

6   [a]*School of Chemical and Process Engineering, University of Leeds, Leeds LS2 9JT, UK.*

7   [b]*School of Earth and Environment, University of Leeds, LS2 9JT, UK.*

8   [c]*School of Electrical and Electronic Engineering, University of Leeds, LS2 9JT, UK.*

9   [d]*Sellafield Ltd, Hinton House, Birchwood Park Ave, Birchwood, Warrington WA3 6GR, UK.*

10   *Corresponding authors. Tel: +44 113 343 2790. E-mail address:* alastairtonge@gmail.com; t.n.hunter@leeds.ac.uk

11

12   *Abstract*— In this study, an acoustic backscatter system was used with single broadband

13   transducers utilising narrowband excitation at multiple frequencies of 2.00, 2.25 and 2.50 MHz,

14   to determine the scattering properties of three sizes of glass particles (40, 78 and 212 μm) in

15   liquid suspensions. A calibration procedure was developed to initially measure the transducer

16   constants, and form function and scattering cross-section values were calculated

17   experimentally. Determined values aligned well with theoretical predictions, where viscous

18   absorption was found to be important for the smallest glass particle size. A logarithmic

19   translation of the signal attenuation gave a linear response, with respect to concentration, up to

20   the maximum measured concentration of 125 gl^{-1} for the two smallest glass species. However,

21   attenuation data for the largest species were only linear up to ~40 gl^{-1}, attributed to significant

22   multiple particle scattering causing an increase in the noise floor. Additionally, a procedure

23   was developed to fit measured attenuation data to a nearfield correction factor correlation,

24   improving measurements in restricted geometries and highly attenuating suspensions.

25   Concentration profiles were produced using both single and dual frequency inversion methods

26   and were found to be accurate up to ~25–40 gl^{-1}, after which multiple scattering effects caused

27   errors in the measured backscatter, and instability in the inverted profiles. Additional scatter

28   observed in the dual frequency inversions was modelled in terms of the ratio between the

29   attenuation coefficients at each frequency and compared to the experimental error. A ratio < 0.6

30   between the attenuation coefficients is suggested to sufficiently minimise errors in the dual

31   frequency inversion.

32

33   *Keywords*:

34   Acoustic Backscatter; Suspensions; Sediment; Particle characterisation; Concentration
35   measurement; Rayleigh scattering.

1   Introduction

37   The monitoring of suspended sediment size and concentration is of great importance for both

38   environmental and engineering purposes. For example, in fluvial and coastal environments,

39   physical sampling can become impractical due to natural turbulence and high flow rates

40   limiting the spatiotemporal resolution of the measurements [1]–[4]. Likewise, engineering

41   processes typically have restricted access or large costs associated with sampling due to either

42   the hazardous nature of the processes or the materials used, such as in nuclear waste treatment

43   [5], [6]. Thus, there is a critical need for remote, flexible techniques for monitoring particle

44   concentration in aqueous environments that are also robust to changes in particle properties, as

45   well as hardware and analysis methods that minimise space requirements in restricted

46   environments [7]–[11].

47

48   Acoustic backscatter systems (ABS) and Doppler profilers are used routinely to study sediment

49   transport in coastal and estuarine environments [12], where concentration information can be

50   gained from the intensity of the backscattered signal at different echo distance points from the

51   transducer [13], [14]. While current characterisation methods are adequate for dilute granular

52   sediments, there are important analytical limitations with fine or polydisperse particles, and

53   also critically, in concentred suspensions of relevance to engineering systems, such as

54   multiphase mixing and separation operations [11]. According to single (dilute limited)

55   scattering models, as derived by Thorne and Hanes [12], if particle scattering properties remain

56   constant with distance, the decay of the acoustic signal caused by the sediment should vary

57   linearly on a logarithmic scale with concentration, where the sediment attenuation coefficient,

58   ξ, should be an intrinsic particle property. The limit of this predicted relationship has been a

59   subject of study for many groups [6], [15]–[22]. At high concentrations, inter-particle distances

60   decrease and multiple scattering effects are enhanced, causing deviation in the attenuation

61   response. These functional changes are not able to be analytically quantified currently,

62   significantly limiting the application of acoustics as concentration profilers. For example, non-

63   linearity between attenuation and concentration was observed by Hipp *et al.* [23] to become

64   more pronounced at low particle sizes and frequencies, where viscous attenuation dominates.

65   However, a fuller understanding of the particle concentration and size limits where multiple

66   scattering dominates is lacking.

67

68   For scattering attenuation, which is the increasingly dominant mode of attenuation as the

69   product of the acoustic wavenumber, k, and the particle radius, a, increases toward unity [24],

70   it was found by Shukla *et al.* [25] that for glass beads of ~ 40 – 120 μm in oil and water using

71   broadband transducers, the attenuation increased linearly with concentration up to 6 %v/v for

72   the largest particle size and up to 18 %v/v for the smallest particle size, highlighting the size

73   dependency of the multiple scattering limit. Multiple scattering has also been shown to cause

74   spreading of the acoustic signal over the time-domain [26], as found by Page *et al.* [27] for

75   measurements through packed beds of glass beads, where the received pulse was spread over

76   a much larger time domain, suggesting longer path lengths travelled by the multiple scattered

77   wave. As ABS uses a fixed sound velocity to convert the time-domain signal into distance,

78   multiple scattering would lead to additional signal components that may increase the overall

79   noise in the system. It would therefore be invaluable to determine an optimal particle size and

80   frequency for which the linear relationship between attenuation and particle concentration is

81   maximised, such that scattering attenuation is the dominant mechanism and the signal is not

82   overly diminished through multiple scattering. These limits may be more readily avoided by

83   using broadband transducers pulsed over different narrowband ranges, for which the

84   measurement frequency can be adjusted, and so their application is also of great interest.

85

86   Quantitative analytical models that relate the backscattered acoustic signal received by an

87   active piezoelectric transducer [12], [28] to characterise the concentration of particles in

88   suspensions have been developed by a number of previous authors [2], [19], [29]–[33]. While

89   a range of methods exist to average received signal peak intensity against particle level ([7],

90   [10]), these do not provide a means to profile with distance, although they may provide an

91   additional estimate for the average concentration that can be used to constrain results from a

92   comparative measurement. For profiling techniques, in summary, if the backscatter and

93   attenuation coefficient parameters of a suspension are known or can be estimated, then a

94   particle concentration profile can be produced using either single frequency [12] or dual

95   frequency inversion methods [34]. The advantage of multi-frequency methods are that they

96   eliminate numerical instabilities in the farfield, normally associated with other inversion

97   approaches [2], [29], [30]. Nevertheless, the use of multi-frequency techniques normally

98   requires multiple discrete probes, which considerably limits their application in restricted

99   engineering environments, and issues may arise if transducers cannot be collocated. As an

100   alternative, it may be possible to utilise broadband probes that can be pulsed at multiple

101 frequencies, provided a sufficient difference in attenuation is observed between the
102 measurement frequencies [8]. In general, research is required to provide a greater
103 understanding of the limitations of both prediction of acoustic constants and subsequent
104 concentration inversion for non-cohesive sediment using ABS.

105

106 Therefore, in this study, a calibration method proposed by Rice *et al.* [8] with the subsequent
107 modification by Bux *et al.* [35], was used in order to find the backscatter cross-section, χ, and
108 form function, *f,* of a range of glass dispersions. The method is straightforward and requires
109 only a few measurements at known, homogeneous concentrations. It also provides a means to
110 study the change in acoustic attenuation with sediment concentration so that results can be
111 compared with existing literature [17], [36]. Values for *f* and χ were determined for three sizes
112 of glass spheres and three frequencies by pulsing broadband transducers at +/- 10 % of the
113 central frequency, in order to assess their ability to accurately observe changes in acoustic
114 constants over their available bandwidth, thus reducing the space required for additional
115 telemetry. The form function and scattering cross-section were then compared to values
116 determined using the heuristic model from Betteridge *et al.* [37] in conjunction with Urick's
117 model for viscous absorption [38]. The backscatter voltage responses were inverted to produce
118 concentration profiles using the single frequency method given by Thorne and Hanes [12] and
119 the dual frequency inversion originally proposed by Bricault [39] that has been utilised
120 previously by Hurther *et al.* [34] and Rice *et al.* [8] for similar systems. However, the use of
121 dual frequency inversions have not yet been applied to single broadband transducers pulsed at
122 multiple frequencies, which could critically increase the amount of data obtained for a given
123 amount of hardware/telemetry space. A novel method for determining the nearfield correction
124 factor that corrects the ABS response close to the probe is also demonstrated and applied to
125 inversion results, to improve fits for space-restricted geometries, such as pipe flows.

126

127 ## 2   Measurement principle and acoustic modelling

128 The following model (Eqn. 1) as presented by Thorne and Hanes [12], gives the variation of
129 acoustic backscattered voltage, *V,* with distance from the transducer face, *r,* for a given mass
130 concentration of suspended particles, *M,* for single particle scattering. Here additionally, k_s is
131 the particle backscatter constant that describes the backscattering strength of the particle
132 species, α_s is the particle attenuation constant, α_w is the attenuation due to water, ψ is the near

133   field correction factor (NFCF) and k_t is the transducer constant, which captures the inherent

134   gain of the system and probe characteristics.

$$V(r) = \frac{k_t k_s M^{\frac{1}{2}}}{r\psi} e^{-2r(\alpha_w + \alpha_s)}$$ 1

135   Physically, the pre-exponential term encompasses the portion of the wave that is reflected at

136   180° back to the transducer, while the exponential represents the portion of the signal that is

137   attenuated by the fluid and sediment. The nearfield correction factor (the limit of which is unity

138   in the farfield) can be estimated using the correlation given by Downing et al. [40] (Eqn. 2)

139   that describes the non-spherical spreading of the acoustic signal in the transducer nearfield, r_n

140   (Eqn. 3), in terms of the ratio of the measurement distance to the nearfield distance, z (Eqn. 4).

141   Here, additionally, a_t is the transducer radius and λ is the wavelength of the ultrasonic signal.

142   There exists some debate over the mathematical definition of the nearfield distance of

143   ultrasonic transducers with various prefactors suggested for the $\frac{a_t^2}{\lambda}$ term [41]. The prefactor of

144   π was selected here as results were to be compared to those produced by Downing et al. [40].

145   Results presented in Section 3.3 indicated that the error fell close to zero at $z = 1$ using this

146   definition for the nearfield, and so it has been assumed to be sufficiently accurate for the

147   analysis procedure.

$$\psi = \frac{1 + 1.35z + (2.5z)^{3.2}}{1.35z + (2.5z)^{3.2}}$$ 2

$$r_n = \frac{\pi a_t^2}{\lambda}$$ 3

$$z = \frac{r}{r_n}$$ 4

148   The particle species backscatter constant (k_s) can be found using Eqn. 5, where a is the particle

149   radius, ρ_s is the particle density and f is the dimensionless form function. Here, the angled

150   brackets indicate a number averaged over the particle size distribution.

$$k_s = \frac{\langle f \rangle}{\sqrt{a\rho_s}}$$ 5

151   The attenuation due to water at zero salinity, α_w (in m^{-1}) is defined by Rice et al. [8] derived

152   from equations by Ainslie and McColm [42] and is shown in the Electronic Supplementary

153   Materials (ESM) Eqn. S.1. The sediment attenuation constant, α_s (also in m^{-1}) is given by

154   Thorne and Hanes [12] (Eqn. 6).

$$\alpha_s = \frac{1}{r}\int_0^r \xi(r)M(r)dr \qquad \qquad \textbf{6}$$

155   Here, ξ (in m^2 kg^{-1}) is the concentration independent sediment attenuation coefficient, as

156   expressed in Eqn. 7, where χ is the dimensionless normalised total scattering cross-section.

$$\xi = \frac{3\langle\chi\rangle}{4\langle a\rangle\rho_s} \qquad \qquad \textbf{7}$$

157   Heuristic expressions for f and χ have been determined previously for spherical glass beads by

158   Betteridge *et al.* [37] (see ESM, Eqns. S.2 and S.5) in terms of the acoustic wavenumber, k, of

159   the ultrasound and the particle radius, a. This set of equations assumes that no multiple

160   scattering occurs, such that the signal reflected from each particle is not affected by the

161   neighbouring particles.

162

163   If viscous losses are to be accounted for when $ka << 1$, then Urick's model [38] can be used

164   to calculate an additional attenuation term, χ_{sv}, caused by visco-inertial interactions between

165   the particles and surrounding fluid. The additional viscous cross-section term is shown in Eqn.

166   8, in terms of the density ratio between the spheres and the surrounding fluid (γ) and $\beta =$

167   $\sqrt{\omega/2\nu}$ and represents the inverse of the viscous boundary layer thickness, ω is the acoustic

168   angular frequency and ν is the kinematic viscosity of water.

$$\chi_{sv} = \frac{2}{3}x(\gamma-1)^2\frac{\tau}{\tau^2 + (\gamma+\theta_v)^2} \qquad \qquad \textbf{8}$$

$$\tau = \frac{9}{4\beta a}\left(1 + \frac{1}{\beta a}\right) \qquad \qquad \textbf{9}$$

$$\theta_v = \frac{1}{2}\left(1 + \frac{9}{2\beta a}\right) \qquad \qquad \textbf{10}$$

$$\chi = \chi_{ss} + \chi_{sv} \qquad \qquad \textbf{11}$$

169   By using heuristically or experimentally determined values of f and χ, and accounting for

170   viscous attenuation when it is significant compared to the sediment and water attenuation,

171   Eqns. 5 - 7 can be substituted into Eqn. 1, leaving only the transducer constant, k_t, as an

172   unknown. Acoustic measurements on homogeneous suspensions of particles at fixed low

173   concentrations with known scattering properties can then be used to find k_t, using Eqn. 12

174   (detailed by Betteridge *et al.* [37]).

$$\frac{r\psi V(r)}{k_s\sqrt{M}}e^{2r(\alpha_w+\alpha_s)} = k_t \qquad \text{12}$$

2.1   *G-function* modelling

In order to be able to determine the attenuation coefficient in arbitrary suspensions, previous authors [1], [8], [43], [44] have linearised Equation 1 with respect to distance, by taking the natural logarithm of the product of the measured voltage, V_{rms}, and the distance from the transducer, r, to produce the '*G-function*' (as denoted by Rice *et al.* [8]) and shown in Eqn. 13.

$$G = \ln(\psi r V_{rms}) = \ln(k_s k_t) + \frac{1}{2}\ln M - 2r(\alpha_w + \alpha_s) \qquad \text{13}$$

Where α_w and α_s are the attenuation due to the water and sediment respectively and k_s and k_t are the backscatter and tranducer constants. If the particle concentration, M, does not change with distance from the transducer, r, the derivative with respect to r gives Eqn. 14.

$$\frac{\partial G}{\partial r} = -2(\alpha_w + \alpha_s) \qquad \text{14}$$

With the requirement that such a relationship only holds for a homogenously mixed system. Applying this same condition to Eqn. 6 gives Eqn. 15, where ξ again is the concentration independent attenuation coefficient.

$$\alpha_s = \xi M \qquad \text{15}$$

Substituting Eqn. 15 into 14 and differentiating with respect to the mass concentration, M, produces Eqn. 16.

$$\xi = -\frac{1}{2}\frac{\partial^2 G}{\partial M \partial r} \qquad \text{16}$$

Thus, by taking the gradient of G plotted against distance, $\frac{\partial G}{\partial r}$ can be determined at multiple concentrations for a given particle system. This derivative can then be plotted against concentration, where the gradient of the linear fit is used to determine ξ via Eqn. 16.

A procedure following the *G-function* method is also given by Bux *et al.* [35] for calibration of the transducer constant, k_t, for any transducer types, k_s. The method uses measured values of attenuation coefficients in well characterised spherical glass dispersions and heuristic expressions for the form function, f, such as that provided by Betteridge *et al.* [37] (e.g. ESM, Eqn. S.2). Once k_t is defined for specific transducers, attenuation and scattering coefficients

197   can be found for any arbitrary suspensions, allowing estimation of concentration profiles using

198   inversion methods.

199

2.2   Single frequency inversion

201   To convert the raw backscattered signal (V_{rms}) to a mass concentration, Eqn. 1 must be solved

202   for M. If only one frequency is available, an estimate must be made for the average particle

203   size ,$<a>$, to allow the backscatter constant, k_s, and the attenuation coefficient, ξ, to be

204   calculated using Eqns. 5 and 7. As long as the transducer constant, k_t, is known and $M\xi \ll 1$

205   then α_s can be assumed to be zero yielding the relationship [12].

$$M_0 = \left\{ \frac{V_{rms}\psi r}{k_s k_t} \right\}^2 e^{4r\alpha_w} \qquad \textbf{17}$$

206   As all terms on the right are known, a concentration profile can be produced. If it cannot be

207   assumed that $\alpha_s \approx 0$ then an iterative approach is used. The first calculation is performed

208   assuming $\alpha_s \approx 0$ the result of which is fed into Eqn. 18 to predict a new value for M,

$$M_1 = M_0 e^{4r\alpha_s} \qquad \textbf{18}$$

209   where α_s is obtained using the newly found M_0 profile. This process is repeated until M_n and

210   M_{n+1} are convergent. This is known as the implicit iterative approach. Caution must be used

211   as the iterative feedback between M and α_s is positive and can cause the solution to diverge to

212   zero or infinity due to feedback errors as the distance from the transducer increases [12].

213

2.3   Dual frequency inversion

215   If two frequencies are available, then a dual-frequency approach can be adopted to eliminate

216   the cumulative error associated with the single-frequency approach [12]. The model, as

217   described by Rice *et al.* [8], is shown in Eqns. 19-24. Eqn. 19 essentially gives the squared

218   form of Eqn. 1 simplified to two terms, *J(r)* and $\Phi^2(r)$. The *J(r)* term (Eqn. 21) contains the

219   sediment attenuation coefficient, ξ, and mass concentration, *M*, while $\Phi^2(r)$ (Eqn. 20),

220   contains the sediment backscatter and transducer constants, k_s and k_t, the attenuation due to

221   water, α_w, and the nearfield correction factor ψ.

$$V^2(r) = \Phi^2(r)J(r) \qquad \textbf{19}$$

$$\Phi^2(r) = \left(\frac{k_s k_t}{\psi r} \right)^2 e^{-4r\alpha_w} \qquad \textbf{20}$$

$$J(r) = Me^{-4\int_0^r \xi(r)M(r)dr} = \frac{V^2(r)}{\Phi^2(r)} \qquad \text{21}$$

222   If the particle size, and therefore ξ and k_s, do not change with distance from the probe, then

223   the attenuation coefficient can be moved outside of the integrals, giving Eqn. 22.

$$J_i(r) = Me^{-4\xi_i \int_0^r M(r)dr} \qquad \text{22}$$

224   Where $i = 1, 2$ for probe frequencies 1 and 2 (2.00 and 2.50 MHz in this study). Dividing Eqn.

225   22 by M, taking the natural logarithm and dividing by ξ_i yields Eqn. 23.

$$\left(\frac{J_1}{M}\right)^{\xi_2} = \left(\frac{J_2}{M}\right)^{\xi_1} \qquad \text{23}$$

226   Finally, rearranging for M gives Eqn. 24.

$$M = J_1^{\left(1 - \frac{\xi_1}{\xi_2}\right)^{-1}} J_2^{\left(1 - \frac{\xi_2}{\xi_1}\right)^{-1}} \qquad \text{24}$$

227   For this method, the attenuation ratio ξ_1/ξ_2 must be sufficiently different from unity to prevent

228   mathematical instabilities and subsequent errors. A single broadband transducer could

229   therefore possibly be used for quasi-simultaneous measurement in co-located sample volumes,

230   when pulsed with narrowband excitation at multiple frequencies. However, the attenuation

231   coefficient must be measured at each frequency and be sufficiently different to have an the

232   accurate and stable inversion [34], which is a critical focus of investigation in this study.

233

234   An equation for calculating the relative (mean-normalised) error in the dual-frequency inverted

235   concentration, $\frac{\delta M}{M}$, in terms of the attenuation ratio and relative error in the measured scattering

236   constant at a single frequency, $\frac{\delta K_1}{K_1}$, has been derived previously by Rice $et\ al.$ [8] (ESM, Eqns.

237   S.7-S.20) and is extended here to include the relative error at the second frequency $\frac{\delta K_2}{K_2}$. The

238   result is shown in Eqn. 25. As the ratio ξ_1/ξ_2 approaches unity, then the terms inside the bracket

239   will approach infinity causing mathematical instabilities in the concentration inversion.

240

$$\frac{\delta M}{M} = \sqrt{\left(-2\left(1 - \frac{\xi_1}{\xi_2}\right)^{-1}\left|\frac{\delta K_1}{K_1}\right|\right)^2 + \left(-2\left(1 - \frac{\xi_2}{\xi_1}\right)^{-1}\left|\frac{\delta K_2}{K_2}\right|\right)^2} \qquad \text{25}$$

241

3   Materials and methods

3.1   Materials characterisation

244   Three sizes of spherical glass beads (Honite 22, Honite 16 and Honite 12) purchased from
245   Guyson International Ltd, UK [45] were used as test materials. They are ideal acoustic
246   scatterers and both heuristic expressions [37] and experimental methods [8], [35] exist to
247   determine their acoustic scattering and attenuation properties. Particle size was measured using
248   a Mastersizer 2000T (Malvern Panalytical Ltd., UK) with median (d_{50}) values of 40, 78 and
249   212 μm given in Table 1 (size distributions are shown within the ESM, Fig. S.1). The size
250   distributions are relatively monodisperse as indicated by the small coefficient of variation,
251   (*COV,* the standard deviation divided by the mean) for each size.

252

253   **Table 1 Median particle size data and variation statistics for the particles used in this study.**

Material Name	Particle d_{50} (μm)	Coefficient of Variation
Honite 22	40	0.31
Honite 16	78	0.29
Honite 12	212	0.27

254

255   In order to confirm the morphology of the glass species, scanning electron microscopy (SEM)
256   images were taken using a TM3030 Plus desktop SEM (Hitachi High-Technologies
257   Corporation, Europe) and are shown within the ESM, Fig. S.2. Although small surface defects
258   and shape deviation are evidenced, the glass particles are observed to be highly spherical.

259

260   ## 3.2   Experimental methodology

261   The acoustic backscatter system used was a bespoke device developed at the University of
262   Leeds; the Ultrasound Array Research Platform (UARPII-16), featuring 16 individual
263   transducer connections [46]. A high measurement speed is necessary to achieve real-time
264   measurement to reduce the time averaging effects inherent in taking the root mean square of
265   multiple measurements. The data path within the instrument is pipelined such that while a
266   measurement is in progress, received data is stored in local memory in real-time while prior
267   measurements can be downloaded from the instrument for analysis [47].

268

269   The UARP modules are built around an Altera Stratix V field-programmable gate array
270   (FGPA) and feature commercial off-the-shelf transmit and receive front end integrated circuits
271   [48]. The transmit signal used was a switched mode waveform, with five discrete voltages of
272   -96V, -48V, 0V, 48V and 96V. Through the use of Harmonic Reduction Pulse Width

273   Modulation (HRPWM) an excitation waveform with reduced harmonic content and time-

274   varying frequency and amplitude can be made.

275

276   The receive path is based around integrated analogue front-end circuits, combining multi-stage

277   amplification, filtering and analogue to digital conversion. High speed serial digital data is

278   received by the FGPA and stored in local memory [48]. The UARP is controlled using a custom

279   MATLAB (Mathworks, USA) interface. All raw data was processed in real-time for operator

280   feedback and archived for further offline processing [49].

281

282   Eight identical immersion transducers with a 2.25 MHz central frequency and 0.25 in.

283   (63.5 mm) diameter elements were tested (Olympus NDT V323-SM). As an example of the

284   system scattering regime, the corresponding ka values for each glass particle size studied, when

285   insonified at the central 2.2.5 MHz frequency, are 0.19, 0.37 and 1.01, for the 40, 78 and

286   112 µm particles respectively. A Harmonic Reduction Pulse Width Modulation (HRPWM)

287   algorithm was used to create three separate transmit waveforms in turn, with local central

288   frequencies of 2.00, 2.25 and 2.50 MHz, each with Hann windowing and a 5 µs duration. The

289   received echo voltage was recorded using 31172 points spaced over the 0.3 m range with

290   10,000 repeat measurements made over a 5-minute period, resulting in a ~85 dB noise floor

291   after signal processing. An example of the excitation signal for the central 2.25 MHz frequency,

292   as well as an example of the time-domain received signal (for the case of 78 µm particles at a

293   nominal concentration of 2.5 g/l) are shown within the ESM (Fig S.3).

294

295   The transducers were placed in an impeller-agitated, 0.8 m tall, 0.3 m diameter calibration

296   arranged radially, facing perpendicular to the tank base, with the experimental setup illustrated

297   schematically in Figure 1 (a further image of the system is shown within the ESM, Fig. S.4).

298   A pump was used to recirculate settling suspension from the conical base of the tank to a

299   manifold arranged at the top of the tank, to prevent particles from settling out and ensure good

300   levels of mixing. Suspension samples were taken at three depths simultaneously using a multi-

301   headed peristaltic pump, and particle concentrations determined gravimetrically (see the ESM,

302   Fig. S.5), where good homogeneity was evidenced for all nominal concentrations.

303   Measurements taken at eight nominal particle concentrations ranging from 2.5 to 133.7 g l^{-1}.

304

305
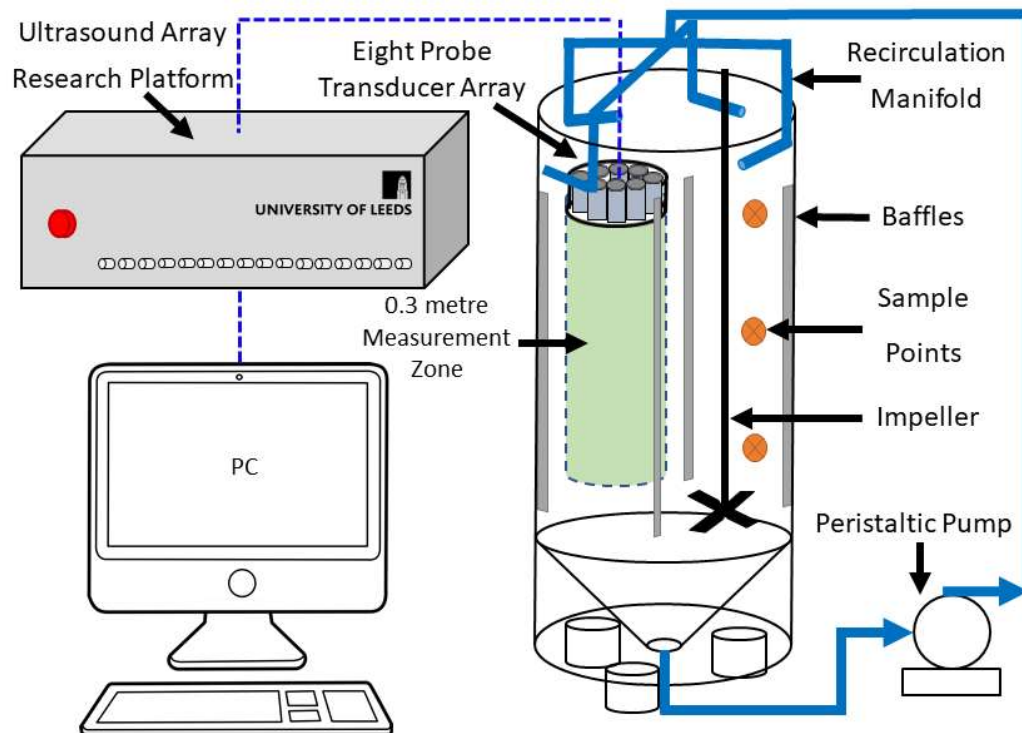
Figure 1: Schematic of the experimental setup used for acoustic backscatter measurements, where the crossed orange circles indicate sample points and grey bars represent the location of baffles.

3.3   Acoustic analysis

In order to determine the acoustic attenuation constant, ξ, and subsequently the scattering cross section, χ and form function, f for each glass species, the extended *G-function* method [8], [35] was applied (Eqns, 13–16). A flowsheet is given within the ESM (Fig. S.6) that demonstrates this procedure.

To improve results in the nearfield (taken as 14–50 mm from the probe face), an alternative correction factor, ψ_G, to that proposed by Downing *et al.* [40] was modelled. Here, ψ_G was calculated on the basis that the resultant *G-function* profile (given by Eqn. 13) would maintain the expected linear relationship predicted by dG/dr, when using the newly modelled ψ_G in place of ψ. The same form of the equation proposed by Downing *et al.* [40], in terms of the ratio of the measurement distance to the nearfield distance, was used to fit the model parameters (a_n) to minimise the objective function, H, shown in Eqn. 26. A numerical fitting procedure was performed using MATLAB, with a non-linear least squares fit (where subscripts i and j indicate each concentration and insonification frequency respectively). A lower and upper bound of 0.1 and 10 were used for the model parameters, and initial values for each variable were identical to those in the original model (Eqn. 2).

$$\sum_{i,j}^{n}\left[exp\left(\frac{dG_{ij}}{dr}r + c_{ij}\right) - V_{ij}r - \frac{a_1 + a_2z + (a_3z)^{a_4}}{a_2z + (a_3z)^{a_4}}\right] = H \qquad 26$$

326

327 Single and dual frequency concentration profiles were inverted from experimental data using
328 Eqns. 17 - 18 and Eqns. 19 – 24, as described. For the single inversions, only a single iteration
329 was undertaken, with the initial guess for the concentration set to be equal to the nominal
330 particle concentration (confirmed from sample data). For the dual-frequency concentration
331 inversions presented in Section 4.3, individual discrete frequency data were analysed and
332 averaged together for the total measurement times, using the method presented in Section 2.3.
333

334 ## 4   Results and discussion

335 ### 4.1   Determination of acoustic constants and near field correction factor
336   modelling

337 Examples of typical decibel profiles for a single probe collected with the UARP, are shown in
338 Figure 2 (a)-(c) for all three particle sizes at three concentrations; measured using the central
339 frequency of the transducer (2.25 MHz). Once outside of the near field (~0.05 m from the
340 transducer) a logarithmic decay of the signal with distance (on a decibel scale) is observed.
341 This relationship is governed by both scattering and attenuation parameters (Eqn. 1). On a
342 decibel scale ($dB = 20\ log_{10}\ (V_{RMS})$) the negative linear slope with distance is determined by
343 the attenuation parameters and the logarithmic decay by the inverse relationship between
344 voltage and distance, typical of moderately attenuating suspensions [19].
345
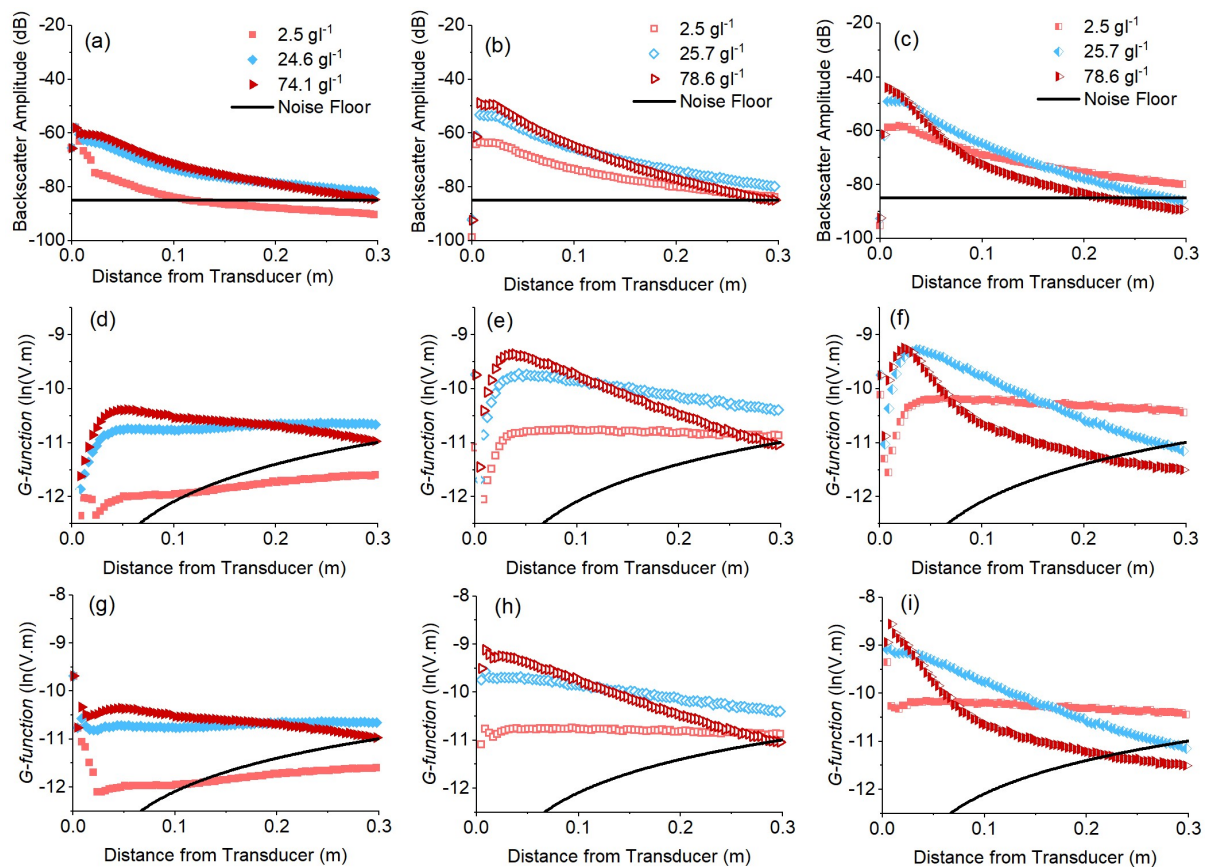
Figure 2: Acoustic backscatter profiles (a) – (c), uncorrected *G-function* translations (d) – (f), and corrected *G-function* translations using fitted Nearfield Correction Factor (NFCF) (g) – (i), for 40, 78 and 212 μm glass particles at three concentrations. Data are for the central 2.25 MHz frequency.

Using Eqn. 13, the backscatter signals were converted to *G-function* values and are shown in Figure 2 (d)-(f). The expected linear relationship between the *G-function* and distance is observed outside of the near field, confirming the homogeneity of the system [8]. Within the nearfield (*r < 0.05 m*) there is a significant reduction in values at distances close to the transducer when no near field correction factor is applied, due to non-spherical spreading of the acoustic signal causing backscattered power to be reduced [40]. Very small positive *G-function* gradients are also seen for the lowest concentration of 40 μm glass beads, likely due to a low signal to noise ratio, caused by the decreasing backscattering constant, k_s, as particle size is decreased [12]. For the 212 μm glass particles and concentrations above ~70 g l^{-1}, there is a notable change in the gradient of the *G-function* with distance at ~0.09 m. It would appear from results presented here that non-linearity of the backscattered signal with distance occurs below a *G-function* value of around -11. Below this value, it is assumed that the signal approaches the instrument noise floor, causing the non-linearity observed in the *G-function*. Indeed, a decrease in the signal-to-noise ratio with increasing concentration (and hence attenuation) has been observed previously by other authors [50], [51] and is attributed to the

14

366   fact that high levels of attenuation will be measured by the transducer as an incoherent signal

367   (i.e. additional noise).

368

369   It is also likely that at high concentrations, inter-particle distance is small enough so that

370   substantial multiple scattering of the compressional wave between particles occur [52]. As the

371   primary mode of attenuation for large particles, where ka approaches 1, is scattering attenuation

372   (as opposed to primarily viscous attenuation as ka approaches zero) then this result may be

373   expected to be most prominent for the largest particle size, as is observed in Figure 2. For the

374   larger particles, the scatter-attenuation will be greater and not limited to the viscous boundary

375   layer width [16] and therefore allowed to propagate through the dispersion, leading to increased

376   system noise and complex decay of the signal with distance. Additionally, spreading of the

377   received acoustic signal over a greater time domain (equivalent to distance in the experimental

378   setup) has also been observed over very short distances (~10 mm) in transmission setups by

379   other authors [26], [27] for large glass beads at high concentrations, as well as in backscattering

380   setups by Tourin *et al*. [53], which may also be contributing to the complex signal decay with

381   distance.

382

383   To improve *G-function* fits in the nearfield, the alternative correction factor, ψ_G, to that

384   proposed by Downing *et al.* [40], was modelled using Eqn. 26. The newly modelled near field

385   correction factor ψ_G (discussed presently in relation to Fig. 3) was used to generate corrected

386   *G-function* profiles, as shown in Figure 2 (g)-(h). The fitted correction factor noticeably

387   improves the profiles in the nearfield region and would therefore allow for more accurate

388   backscatter determination in applications where dispersion attenuation or physical geometry

389   limits the available measurement range. Fig. 3 (a)-(c) shows the fitted data used to produce the

390   ψ_G for all three particle species. Data for certain probes and concentrations were omitted when

391   the data lay outside twice the root-mean square error of the initial model fit. Data above

392   concentrations of ~70 g l^{-1} were also excluded, as they were found to predict significantly lower

393   values for ψ_G compared to other particle sizes and concentrations.
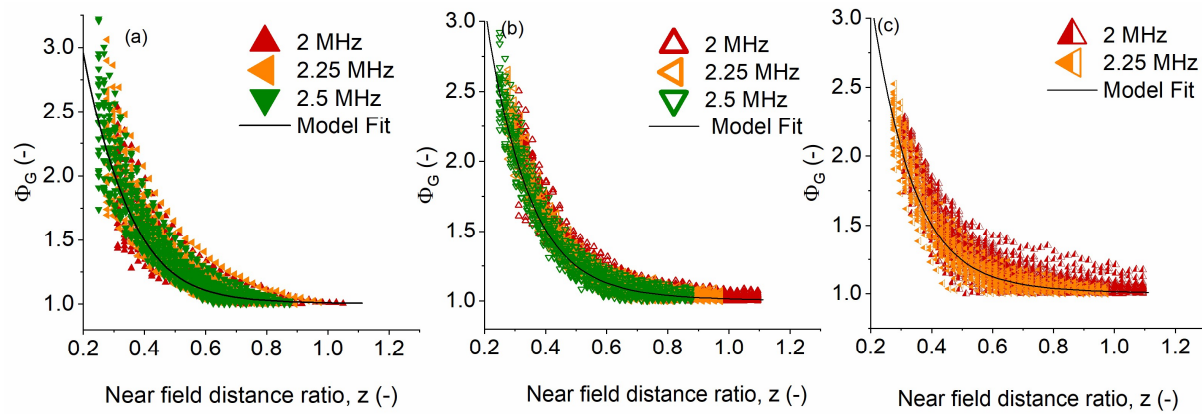
**Figure 3: Fitted Near Field Correction Factor (NFCF) model for (a) 40 µm, (b) 78 µm, and (c) 212 µm glass particles.**

Comparison to the NFCF model proposed by Downing *et al.* [40] (Eqn. 2) is shown in Figure 4. The two models are in general in close agreement, although it can be observed that the modified ψ_G is consistently above the value predicted by the original NFCF. The cause of the deviation is likely due to small imperfections in the transducer shape and surface affecting the nearfield spreading characteristics of the acoustic signal. As expected also, ψ_G does not vary considerably with particle size [40]. In general, because fitting of the model was not computationally intensive and was easily implemented using MATLAB, it is recommended that the NFCF method presented here is incorporated whenever a transducer calibration is performed for a given set of probes, if measurements in the nearfield are to be used for further analysis. This procedure would subsequently improve measurements in zones close to the transducer such as in pipe flow applications [8], [54] and when taking backscatter measurements in highly attenuating or concentrated dispersions [19], [55].
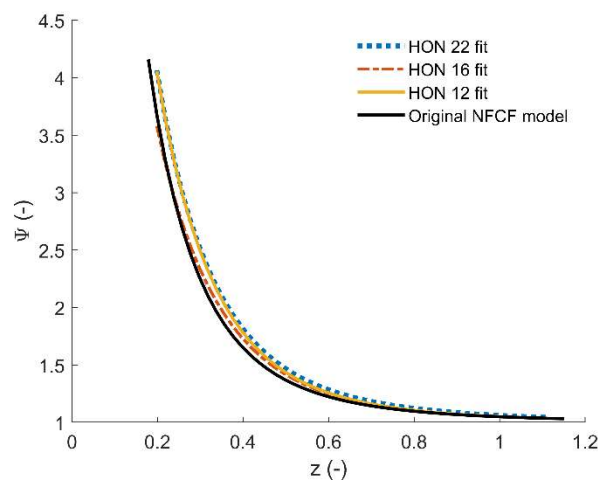

Figure 4: Comparison of fitted NFCF against Downing et al. [40] model for 40, 78 and 212 µm glass particles.

16

413

414   The gradient dG/dr values versus concentration are presented in Figure 5 for the three particle

415   types, with dashed linear interpolations indicating the fits taken to calculate the attenuation

416   coefficient (Eqn. 16). The dG/dr values were determined by assessing the gradient of the G-

417   *function* profiles (Figure 2) between 0.05–0.24 m from the transducer, where the distance range

418   was adjusted if required, to obtain the most negative value for the gradient while maintaining

419   a minimum range of 0.05 m and ensuring that data below the noise floor (set as -85 dB) were

420   excluded. Adjustments were required for the 40 μm glass beads at the lowest concentration,

421   due to the artificial positive gradient, a result of a low signal-to-noise ratio, and for certain

422   systems at high concentrations to mitigate the effect of multiple scattering on the attenuation

423   at greater distances (e.g. the 212 μm glass particles at 78.8 gl^{-1} in Fig. 2).

424

425
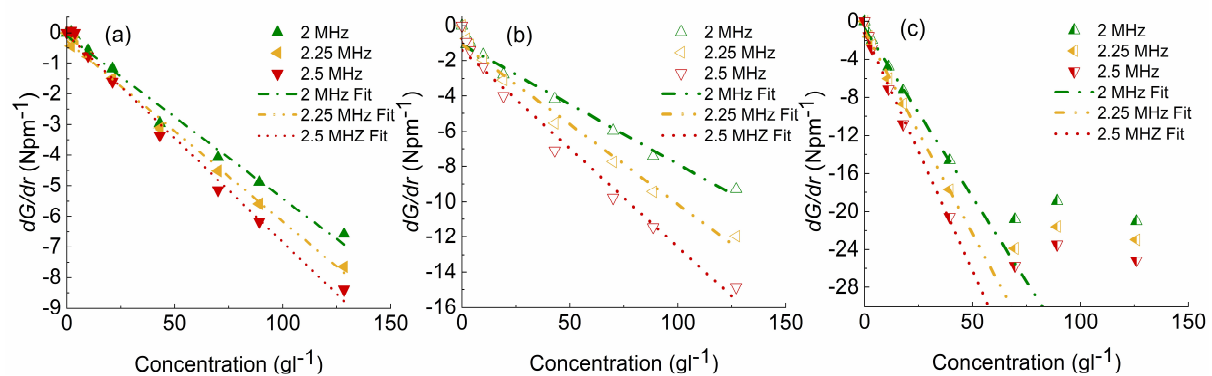
Figure 5: Gradient change in the G-*function* with distance (dG/dr) versus particle concentration for (a) 40 μm, (b) 78 μm and (c) 212 μm glass particles.

428

429   The expected linear gradient is observed with all concentrations for the 40 and 78 μm glass

430   particles and fits generally had R^2 values of ~0.99, while the 212 μm glass particle R^2 value

431   was ~0.92. With respect to the 212 μm glass particles results (Figure 5 (c)), there is a clear

432   concentration limit at which the measured attenuation is no longer proportional to

433   concentration. A similar concentration limit in transmission measurements has been observed

434   by both Stolojanu and Prakash [17] and Atkinson and Kytömaa [36] for glass particles in water,

435   as well as other authors for differing particle systems [23], [25], [56], [57] and is widely

436   attributed to an increase in multiple scattering effects [54]. It is also noted that both authors

437   [23], [32], observed an increase in this non-monotonic behaviour as ka increases towards unity,

438   an effect also observed in the experimental results in Figure 5. As discussed previously in

439   relation to Fig. 2(i), there is additionally a change in the gradient of G-*function* with distance,

440   which may also be an indication of strong multiple scattering effects.

441

442   For a multiple scattered signal to contribute significantly, the signal attenuation (either from
443   non-directional scattering or absorption) must be large when compared to the portion of the
444   signal that is backscattered. If the attenuation due to water is assumed to be small, the
445   exponential term in Eqn. 1 effectively gives the fraction of the signal that is not scatter-
446   attenuated by the sediment and is received by the transducer, while the remaining portion is
447   scattered into the surrounding medium. Therefore, when the value of the exponential term
448   approaches 0 (i.e. when the overall sediment attenuation coefficient is very large) only a small
449   fraction of the acoustic signal is received by the transducer. In these conditions, multiple
450   scattering effects would be expected to become important and would increase with
451   concentration, distance and sediment attenuation, as can be observed in Figure 5 for the large
452   glass. It is important to note that the multiple scattering effects differ in nature to those observed
453   for colloidal dispersions [23], [58], where viscous attenuation dominates and overlap of the
454   viscous boundary layers may cause decreases in attenuation. It is proposed here that the
455   decreasing linearity of attenuation with concentration at high solids loading is caused by
456   incoherent multiple scattering, leading to an increase in the noise floor at greater distances from
457   the transducer, thereby causing the non-linearity of the signal and the observed reduction in
458   attenuation at greater distances.

459

460   Having determined the attenuation coefficients from the straight-line fits in Figure 5, the
461   extended *G-function* method was then applied, where Eqn. 12 was used to obtain profiles of
462   the calculated transducer constant, k_t with distance, for the lowest two particle concentrations
463   (2.5 and 5 g l^{-1}). Nominal concentration values were used in conjunction with the measured
464   attenuation coefficient and a heuristically estimated scattering constant from the Betteridge *et*
465   *al.* [37] correlations as described (ESM, Eqns. S.2–S.6). The k_t profiles were concentration and
466   distance averaged over 0.1-0.2 m from the transducer for the 40 μm and 78 μm glass particles
467   to avoid any potential near field effects and over 0.04-0.1 m for the 212 μm glass particles, due
468   to limitations caused by the higher attenuation. Having found k_t, Eqn. 12 was rearranged so
469   that k_s profiles could be recalculated using the nominal concentration and attenuation
470   coefficient. As k_t and k_s are calculated through the same equations and set of experimental
471   values, they have the same effective profile with distance and are inversely proportional.
472   Example profiles for k_t are provided within the ESM (Fig. S.7) with all k_t values found for each
473   probe, particle size, and frequency, also given for completeness (ESM, Table S.1).

474

475   Figure 6 presents examples of the calculated k_s, as a function of distance for each particle size

476   at the central frequency for a single probe. Although it should be constant with range according

477   to Eqn. 1, k_s increases exponentially with distance at higher concentrations for the 212 μm glass

478   particles, where a less significant, but similar, trend is observed for both the 40 and 78 μm

479   species. A likely factor contributing to this effect is the overall decreased contribution of the

480   scattering term to the backscattered signal when attenuation effects begin to dominate. Small

481   errors or deviations in the estimation of the attenuation coefficient can therefore cause large

482   deviations in the calculation of k_s at high concentrations, as any deviation in ξ will be multiplied

483   through by the concentration value (Eqn. 1). As proposed, multiple scattering may be

484   pronounced for highly scatter-mode attenuating particles, causing the observed attenuation

485   (assumed to be constant for calculation of k_s) to decrease with distance. This effect was

486   observed, in particular, with the *G-function* results for the 212 μm glass particles (Figure 2 (f)),

487   which would subsequently cause the overestimation of the attenuation at greater distances

488   causing the non-linearity in k_s.

489
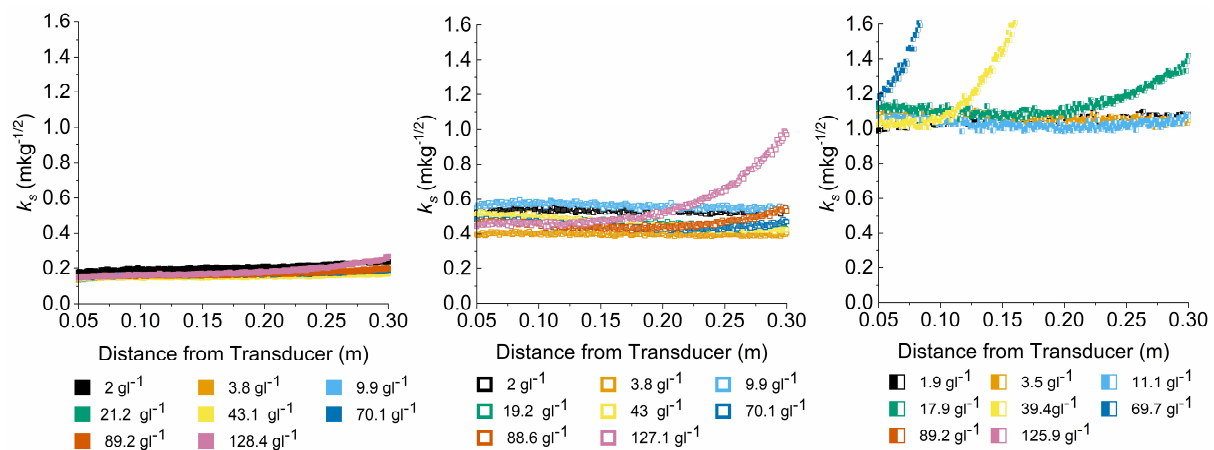
Figure 6: Calculated backscatter coefficient, k_s, versus distance for (a) 40 μm, (b) 78 μm and (c) 212 μm glass particles. Shown are data for the central frequency (2.25 MHz).

4.2   Comparison of particle scattering and attenuation coefficients to model values

496   Figure 7 presents a comparison of the experimental values for the scattering cross-section, χ,

497   averaged over the 8 probes used in the experiments (obtained using Eqns. 7, 14 and 16) to

498   predictions from the heuristic Betteridge *et al.* [37] model, with incorporation of viscous

499   adsorption effects using the model of Urick [38]. The attenuation coefficients from all probes

500   that are used to calculate χ, are given in the ESM (Table S.2). It is observed that viscous

19

501   absorption has very little effect on the overall scattering cross section for the 212 μm glass

502   particles, where $ka \sim 1$, and only a minor effect for the 78 μm glass particles. For the 40 μm

503   glass particles, there is notable improvement in the prediction of the scattering cross-section

504   when viscous losses are accounted for, indicating that viscous losses are large at $ka < \sim 0.6$.

505   Additionally, the measured values for the 212 μm glass particles are slightly below those

506   predicted from the model, which may be due to the influence of the particle size distribution.

507   This trend would be consistent with the work of Thorne and Meral [59], who observed that χ

508   was larger than would be predicted for a uniform size distribution for $ka < 1$ and lower than

509   predicted for $ka > 1$, in moderately polydisperse systems.

510
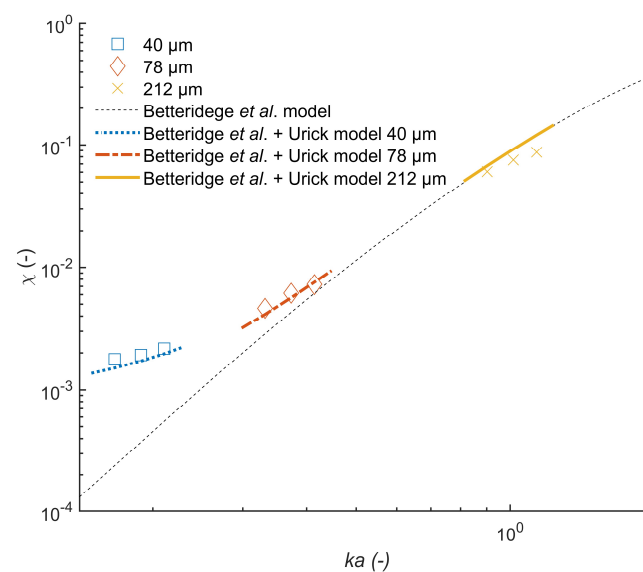
Figure 7: Measured total scattering cross-section (χ) for the three particle species at all frequencies (2, 2.25 and 2.5 MHz) as a function of particle size (a) and wavenumber (k). Includes comparison to the Betteridge *et al.* scattering model [37] in conjunction with Urick's model of viscous attenuation [38].

515   Using Eqn. 5, the form function, f, was calculated based on using a single distance-averaged

516   mean value of k_s from the low concentration experimental data (as shown in Figure 6) and

517   modelled using Eqns. 5 and 12, presented as a function of ka for each particle size in Figure 8.

518   A table giving distanced averaged k_s values for all probes and all concentrations is shown

519   within the ESM, Table S.3, for completeness. A good fit to the Betteridge *et al.* [37] model is

520   again observed, indicating that the *G-function* calibration procedure is valid for calculating the

521   particle backscatter coefficient, k_s. However, it should be noted that there is a level of circularity

522   in k_s measurements, as the value of the transducer constant, k_t, is estimated using the Betteridge

523   *et al.* model [37] to initially estimate k_s. Therefore, the values of k_s, and hence f, would generally

524   be expected to align well with the model. As the particle backscatter coefficient, k_s, is taken as

525   an average value over a particular distance range, deviations from the model shown in Figure

526   8 therefore represent the error due to both scatter in the value of k_s with distance and complex

527   decay of the signal, which subsequently causes distance non-linearity of k_s as observed in

528   Figure 6.

529
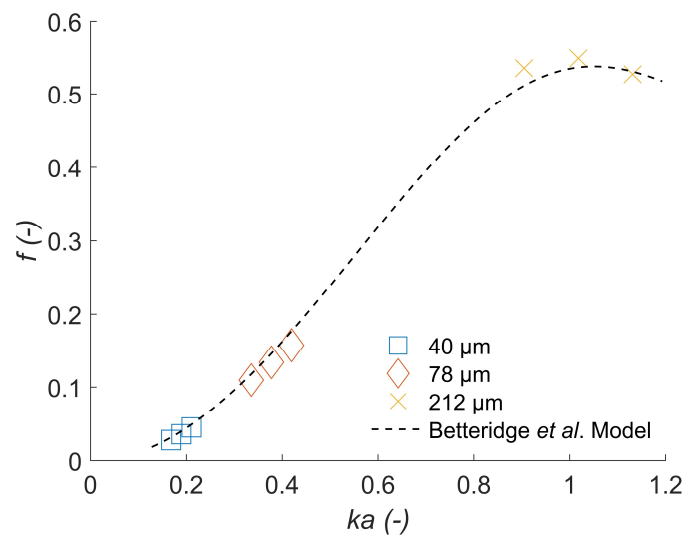
530

531   **Figure 8: Measured form function (*f*) as a function of *ka* for the three particle types at all frequencies (2,**
532   **2.25, 2.5 MHz) in comparison to the Betteridge *et al.* model [37].**
533

4.3   Single and dual frequency concentration inversions

535   In order to determine the experimental limits of the single frequency (Eqns. 17 and 18) and

536   dual frequency inversions (Eqn. 24) concentration profiles were measured for a broad regime

537   in the homogeneously mixed calibration tank. Thus, the mean gravimetrically determined

538   concentration could be used for comparison (i.e. experimentally, there was no deviation in

539   concentration with depth). Individual values of k_s for each concentration were used to account

540   for k_s variation at high concentrations. The same values were used for both the single and dual

541   frequency inversion as the calibration tank was homogeneously mixed and so the particle size,

542   and hence the scattering properties, would not be expected to change with distance [60]. Errors

543   in the concentration profiles would therefore be expected to occur when the calculated k_s profile

544   deviates considerably from the constant value used in the inversion. It is important to note that,

545   as k_s is calculated using experimentally determined values of ξ (using Eqn. 16) any errors in

546   the measured attenuation are reflected in k_s.

547

548   Figure 9 presents the concentration profiles produced using Eqns. 17 and 18 with the
549   experimentally determined nearfield correction factor (ψ_G). There is good agreement with
550   average sample values (within 10%) for the smallest two sizes of glass particle at all but the
551   highest concentrations, at least for moderate distances, while there is an increasing deviation
552   with distance and concentration that is particularly prominent for the largest particle size.
553   Similar results can be found in previous literature [19], [34] and are typically attributed to the
554   fact that, as feedback is positive between the estimated concentration and sediment attenuation
555   term, errors accumulate along the profile causing a solution that diverges to zero or infinity
556   [12]. In contrast, for the data presented here, the gravimetrically measured concentration was
557   used for the inversion calculation at all distances and so this positive feedback is avoided. As
558   concentration and distance from the transducer increase, however, any error in the predicted
559   attenuation coefficient, may be magnified through multiplication with distance and
560   concentration when inverting for concentration (Eqns. 15, 17 and 18) and would contribute to
561   an increasing error. Given that the straight line fits used to estimate the attenuation coefficient
562   were accurate up to the highest measured concentrations for the 40 μm and 78 μm glass
563   particles (see Fig. 5) it is therefore unlikely that a poor fit for estimating attenuation coefficient
564   is the cause of the errors in the inversions for the smaller two particle sizes. The more probable
565   cause is the previously discussed multiple scattering effects at greater concentrations and
566   distances from the transducer (e.g. Figure 2 (f)) [12]. Such a result is not thought to indicate
567   that the physical attenuation decreases at high concentrations and distances, but that multiple
568   scattering presents a concentration limit for the theory used to calculate the scattering and
569   attenuation parameters [8], [12], and results become invalid due to increased system noise.
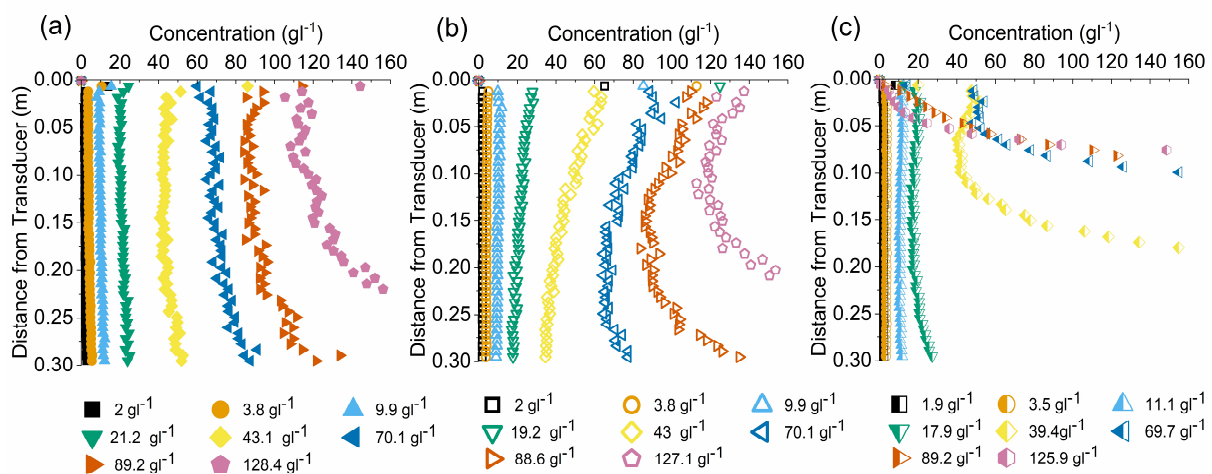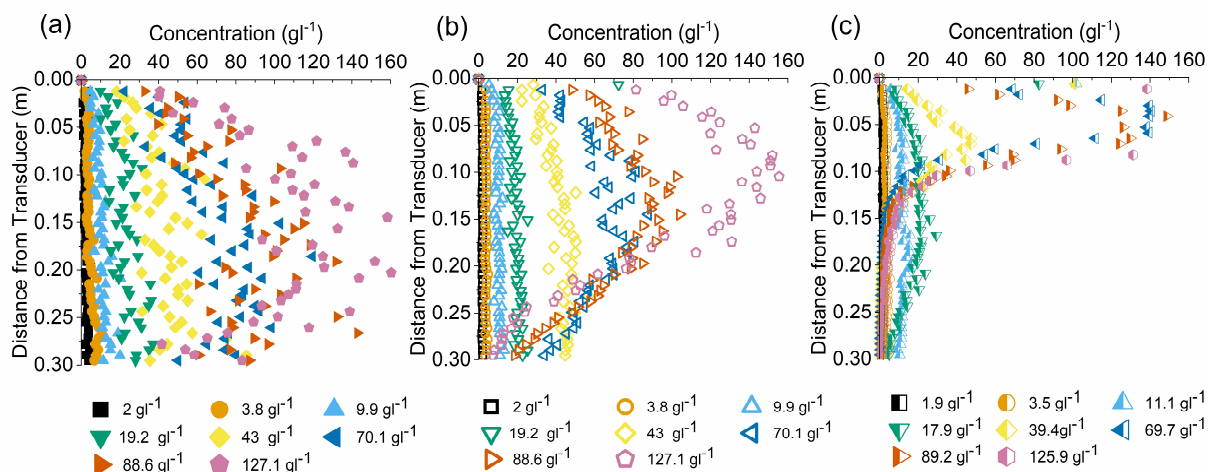

Figure 9: Single frequency inversion profiles for (a) 40 μm, (b) 78 μm and (c) 212 μm glass particles at 2.25 MHz with nearfield correction factor. Legend entries indicate mean samples concentrations.

574   In order to eliminate the propagation of errors along the profile seen in the single frequency

575   inversions, the dual frequency method (as described in Eqns. 19-24) [8], [34], [39]) was applied

576   to the data using the experimentally determined values for k_s and ξ. Figure 10 shows the dual

577   frequency profiles obtained for each particle size at a frequency pairing of 2.00 and 2.50 MHz.

578   The widest frequency spacing was chosen, as this offered the attenuation ratio most different

579   from unity and therefore, it was assumed, the smallest relative error in the concentration

580   inversion according to the relationship derived by Rice *et al.* [8] (Eqn. 25). It is observed that

581   the dual frequency profiles obtain relatively accurate concentration profiles up to ~20 g l^{-1},

582   above which the inversion diverges towards zero. Secondly, above ~20 g l^{-1}, there is scatter

583   that worsens with increasing particle concentration. This random deviation can be predicted

584   using the equation derived by Rice *et al.* [8] (Eqn. 25) and would be expected to increase as

585   the attenuation coefficient ratio $\frac{\xi_1}{\xi_2}$ approaches unity. The additional error introduced by the dual

586   frequency method, as compared to the single frequency inversions, is thus likely caused by

587   insufficient differences in the attenuation coefficients at each frequency. It is also noted that

588   the scatter is much more pronounced for the 40 μm glass compared to the other two particle

589   sizes and may be related to a smaller change in the attenuation coefficient with frequency for

590   the smaller particle. In general, as with the single frequency inversion, concentration

591   predictions for the largest particles are the most poorly aligned. Thus, while using an

592   attenuation ratio produces a more mathematically stable relationship, it cannot overcome

593   significant effects of multiple particle scattering.

594

Figure 10: Dual frequency inversion profiles for (a) 40 μm, (b) 78 μm and (c) 212 μm glass particles with a frequency pairing of 2 and 2.5 MHz. Legend entries indicate mean samples concentrations.

595
596

597

598   In order to fully investigate the accuracy limits of the concentration profiles obtained using the

599   single and dual frequency inversion methods, mean concentration values were compared to the

600   sample values in Figure 11 (a) and (b). Here, the means were averaged over the same distance

601   ranges used to calculate k_t and k_s to minimise both nearfield and multiple scattering effects. In

602   comparison, greater deviation from the gravimetrically measured concentration is evident for

603   the dual frequency inversions (similar to the concentration profiles) where, in general, the

604   single inversions are accurate up to concentrations of ~ 80 g l^{-1}, while the dual frequency

605   inversions are only accurate up to a lower value of 40 g l^{-1}. However, both limits are high

606   enough to be within dispersion concentration regimes of many industrial multiphase mixing

607   and settling systems ([11], [61]), highlighting the potential of ABS as process monitors.
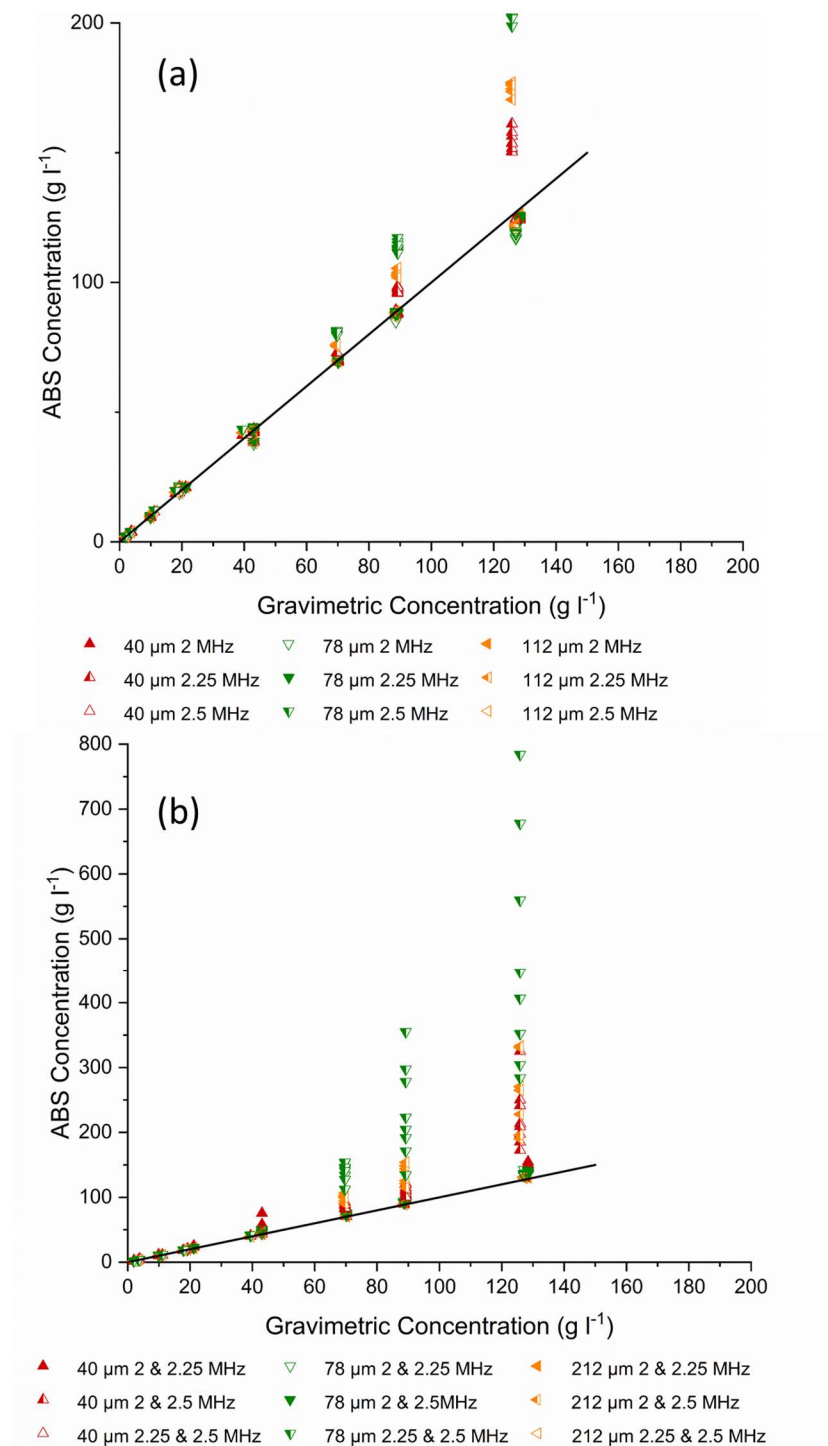
Figure 11: Mean concentration comparisons, as measured by the acoustic backscatter system against values gravimetrically determined, for (a) single frequency and (b) dual frequency inversion models. Solid line displays 1:1 relationship.

In addition to the mean concentrations, the coefficients of variation for the ABS concentration profiles were calculated for each particle size using the single and dual frequency inversion methods over the depth range. Values are shown as a function of the measured sample concentrations within the ESM (Fig. S.8). For the single frequency inversions, a rapid increase

25

617 in the coefficient of variation (COV) is observed for the 212 μm glass particles above 40 g l⁻¹,

618 while the 40 and 78 μm glass particles remain relatively accurate (COV < 0.24) up to 127 g l⁻¹.

619 Furthermore, for the single frequency inversion, the 78 μm glass particles obtains a lower COV

620 than the 40 μm up to 5 g l⁻¹ at 2.5 MHz and up to 10 g l⁻¹ at 2 and 2.25 MHz. This difference is

621 likely a result of the higher signal strength for the 78 μm glass particles as compared to the 40

622 μm glass particles, for which the signal is close to the estimated noise floor (as seen in Fig. 2).

623 In addition, there is a consistent increase in the COV with increasing frequency at

624 concentrations greater than 10 g l⁻¹, again indicative of increased error from multiple scattering

625 effects. Comparing the COV observed in the dual frequency results to the single frequency

626 data, an overall increase in the COV across all particle sizes is observed, except where the mean

627 ABS-measured value is significantly over-estimated (thus also correspondingly decreasing the

628 calculated COV value). It is noted, in general, that the 78 μm glass particles consistently give

629 the lowest COV values of all three particle sizes for the dual frequency inversion and also

630 obtains the most accurate concentration values. This enhancement is thought to largely be a

631 result of the greater difference in attenuation values between the frequencies used, moving the

632 attenuation ratio away from unity.

633

634 To further investigate the scatter in the dual frequency inversions, the equation given by Rice

635 *et al.* [8] (Eqn. 25) was used to compare the measured error in experimental concentration

636 profiles to the error estimated from calculated k_s profiles. Figure 12 presents the error in the

637 measured concentration values, $\frac{\delta M}{M}$, as a function of the attenuation coefficient ratio, $\frac{\xi_1}{\xi_2}$, where

638 solid markers indicate the actual experimental errors for the dual frequency method and the

639 hollow markers correspond to the estimate for the error calculated using Eqn. 25. For each

640 profile, the relative error in the scattering constants at each frequency, $\left|\frac{\delta K_1}{K_1}\right|$ and $\left|\frac{\delta K_2}{K_2}\right|$, and

641 relative error in the concentration, $\frac{\delta M}{M}$, were determined by taking the absolute deviation for the

642 calculated k_s and M profiles and normalising it to the mean value for the profile. The same

643 distance range as that used for k_t was chosen to determine the mean value and relative error of

644 the k_s and M profiles. In order to avoid additional errors from a poor estimate of the attenuation

645 value observed at high concentrations and potential multiple scattering effects, $\frac{\delta M}{M}$ was only

646 calculated for concentrations below 20 g l⁻¹ and averaged to produce the mean error for each

647 probe at each $\frac{\xi_1}{\xi_2}$ ratio (plotted as the empty markers in Figure 12). It is noted that the attenuation

648 ratios associated with the widest frequency bandgap (2.00–2.50 MHz) were used along with

649   the other frequency pairs (2.00–2.25 MHz, 2.25–2.50 MHz) in the error analysis, giving three

650   ratio values for each particle size.

651

652   The estimated error is greater than the observed error in all cases, but does follow a similar

653   trend, with the attenuation coefficient ratio increasing as $\frac{\xi_1}{\xi_2}$ approaches unity. As k_s was

654   calculated by assuming all the other terms in Eqn. 12 remained constant, the error in estimating

655   all these terms is absorbed into the calculated k_s values and hence $\left|\frac{\delta K_1}{K_1}\right|$ and $\left|\frac{\delta K_2}{K_2}\right|$. Errors in

656   other parameters that are assumed constant, such as the attenuation coefficient, will not scale

657   in the same way as errors in k_s and would therefore cause Eqn. 25 to predict values that are

658   offset from the real measured values of $\frac{\delta M}{M}$. Deviation in the experimental values of $\frac{\delta M}{M}$ from

659   the values calculated using Eqn. 25 would therefore indicate that some amount of error is not

660   due to errors in k_s directly, but instead caused by errors in another value that has been assumed

661   constant. Therefore, as the experimental results for the 78 μm glass particles match closely with

662   predicted values, this suggests that the majority of the error was due to small random variation

663   in k_s, likely a result of turbulence in the tank and the moderate size distribution of the glass

664   spheres. This result would therefore imply that the other parameters used to calculate k_s (Eqn.

665   12) i.e. the estimated attenuation coefficients are accurate for the 78 μm data. For the other two

666   sizes of glass particles, conversely, it is clear that there is some degree of error in either the

667   sediment attenuation constant, α_s, or a general deviation from the model, as a result of multiple

668   scattering and increased system noise.

669
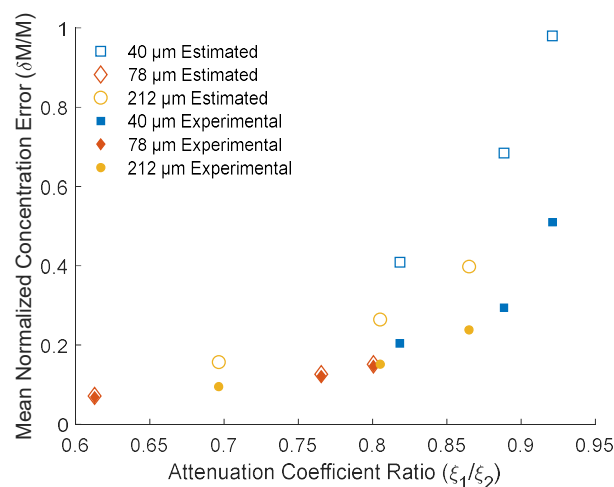
671   **Figure 12: Calculated and experimental mean normalised error in the dual frequency inversion profiles**

672   **($\frac{\delta M}{M}$) for all particle sizes and frequency pairings, as a function of the attenuation coefficient ratio ($\frac{\xi_1}{\xi_2}$).**

673

674   Despite the differences between the measured and predicted error, it is evident that the level of

675   scatter in the dual frequency inversions is generally within expected ranges. This low relative

676   error indicates that, so long as the frequency range is wide enough such that the resulting

677   attenuation coefficient ratio is < ~0.6, a single broadband transducer is able to obtain an

678   accurate dual frequency concentration, using two narrowband measurements. The dual

679   frequency inversion is advantageous compared to the single frequency method, where

680   concentration must be estimated or calculated iteratively causing errors to accumulate in the

681   inversion with distance [34]. Even if the scatter from the dual frequency profile is large, it may

682   provide good initial estimates for the concentration to be secondarily inputted into a single

683   frequency inversion, for a closer refinement. The dual frequency method can also be applied

684   when sediment attenuation coefficients are not known *a priori* (as long as particle k_s values are

685   known explicitly, or can be estimated from their d_{50} size) by taking *dG/dr* gradient values in

686   well mixed systems (or at least in regions where concentration is assumed to be constant) where

687   the sediment attenuation term, α_s, can be found at each frequency. For a region of constant

688   concentration, M, $\frac{\xi_1}{\xi_2}$ is equivalent to $\frac{\alpha_{s1}}{\alpha_{s2}}$, and therefore the ratio can be substituted directly into

689   Eqn. 24 and the dual frequency inversion can be performed.

690

691   5   Conclusions

692   The particle level and *ka* limits of a simple calibration method to determine sediment

693   concentration using acoustic backscatter systems [8], [35], has been explored for three sizes of

694   glass spheres (40, 78 and 212 μm) insonified at 2.00, 2.25 and 2.50 MHz, using 2.25 MHz

695   central frequency broadband probes. The expected trend of increasing scattering cross-section

696   and form function with particle size and frequency were observed, and results compared well

697   with the heuristic model from Betteridge *et al.* [37] when coupled with Urick's model [38] for

698   viscous attenuation. The greatest deviation was observed for the 212 μm glass particles due to

699   the high *ka* value (~1) and the Rayleigh regime limitations of calibration method [8], [35]. An

700   alternative nearfield correction factor was also presented to improve concentration inversion

701   accuracy in the nearfield, based on the correlation originally proposed by Downing *et al.* [40],

702   allowing constricted geometries such as pipes to be profiled.

703

704 Experimentally measured attenuation presented the expected log-linear relationship (using the
705 logarithmic G-*function*) with concentrations up to ~125 g l^{-1} for the two smallest particle
706 systems (*ka* ~0.2 and *ka* ~0.4) and up to ~40 g l^{-1} for the largest, 212 μm, glass particles (*ka*
707 ~1.0). Beyond this limit, the relationship overpredicted the measured attenuation and was
708 attributed to multiple scattering effects causing an increase in the noise floor. Multiple
709 scattering effects were also proposed to be the cause in the apparent reduction of attenuation at
710 longer distances observed for the 212 μm particles. Single frequency inversions were used to
711 generate concentration profiles in well mixed dispersions, and were found to be accurate up to
712 ~125 g l^{-1} for the 78 and 40 μm glass particles and up to ~40 g l^{-1}for the 212 μm glass particles,
713 due to the increase in attenuation with particle size. At high concentrations and distances,
714 multiple scattering effects were again observed to increase the system noise floor, causing
715 significant model deviations.

716

717 To help overcome the mathematical instabilities of the single inversions, a dual frequency
718 inversion method was applied to multiple narrowband pulses using the single broadband
719 transducers (for a maximum 2.00 – 2.50 MHz paring) using the method developed by Hurther
720 *et al.* [34] from preliminary work by Bricault [39], and were shown to be accurate up to ~20
721 g l^{-1}. Above this value, the profiles displayed greater level of scatter when compared to the
722 single frequency inversions. The coefficient of variation in the profiles also increased with
723 concentration, due to greater error in the calculated values of k_s with distance. Additionally, the
724 scatter increased further as the attenuation ratio (ξ_1/ξ_2) became closer to unity, for particle sizes
725 approaching the Rayleigh regime limit. Nevertheless, results presented indicate that for low
726 attenuation ratios ($\xi_1/\xi_2 < $~0.6) the dual frequency inversion was accurate and highlights
727 additional applicability of this method for single broadband transducers. Dual frequency
728 inversions provide a number of advantages for monitoring complex engineering dispersions
729 systems, as they do not require iterative solutions, where the attenuation ratio can be found for
730 many arbitrary particles using the simple calibration procedure presented. Additionally, they
731 provide a greater measure for determining the uncertainty or statistical variation in the
732 experimental parameters used for the inversion. Results overall indicate that the combined use
733 of single and dual frequency inversions using single broadband transducers offers an enhanced
734 methodology for the application of ABS systems as concentration profilers in high
735 concentration dispersions.

Acknowledgements

Example MATLAB code scripts for the acoustic analysis (for the 40 μm particle dataset) have been uploaded to a publicly accessible repository available at: https://github.com/alastair-tonge/acoustic-analysis-of-glass-aprticles-using-broadband-transducers.

References

[1] M. Guerrero and V. Di Federico, "Suspended sediment assessment by combining sound attenuation and backscatter measurements – analytical method and experimental validation," *Adv. Water Resour.*, vol. 113, pp. 167–179, Mar. 2018.

[2] P. D. Thorne and P. J. Hardcastle, "Acoustic measurements of suspended sediments in turbulent currents and comparison with *in-situ* samples," *J. Acoust. Soc. Am.*, vol. 101, no. 5, pp. 2603–2614, May 1997.

[3] P. D. Thorne, D. Hurther, R. D. Cooke, I. Caceres, P. A. Barraud, and A. Sánchez-Arcilla, "Developments in acoustics for studying wave-driven boundary layer flow and sediment dynamics over rippled sand-beds," *Cont. Shelf Res.*, vol. 166, pp. 119–137, 2018.

[4] S. Naqshband, J. S. Ribberink, D. Hurther, P. A. Barraud, and S. J. M. H. Hulscher, "Experimental evidence for turbulent sediment flux constituting a large portion of the total sediment flux along migrating sand dunes," *Geophys. Res. Lett.*, vol. 41, no. 24, pp. 8870–8878, Dec. 2014.

[5] M. S. Greenwood, J. L. Mai, and M. S. Good, "Attenuation measurements of ultrasound in a kaolin–water slurry: A linear dependence upon frequency," *J. Acoust. Soc. Am.*, vol. 94, no. 2, pp. 908–916, Aug. 1993.

[6] J. Bux, N. Paul, T. N. Hunter, J. Peakall, J. M. Dodds, and S. Biggs, "In situ characterization of mixing and sedimentation dynamics in an impinging jet ballast tank via acoustic backscatter," *AIChE J.*, vol. 63, no. 7, pp. 2618–2629, 2017.

[7] R. Weser, S. Wöckel, B. Wessely, and U. Hempel, "Particle characterisation in highly concentrated dispersions using ultrasonic backscattering method," *Ultrasonics*, vol. 53, no. 3, pp. 706–716, 2013.

[8] H. P. Rice, M. Fairweather, T. N. Hunter, B. Mahmoud, S. Biggs, and J. Peakall, "Measuring particle concentration in multiphase pipe flow using acoustic backscatter: generalization of the dual-frequency inversion method.," *J. Acoust. Soc. Am.*, vol. 136, no. 1, pp. 156–169, 2014.

[9] X. Zhan, Y. Yang, J. Liang, D. Zou, J. Zhang, L. Feng, T. Shi, and X. Li, "In-line mixing states monitoring of suspensions using ultrasonic reflection technique," *Ultrasonics*, vol. 65, pp. 43–50, Feb. 2016.

[10] L. Elvira, P. Vera, F. J. Cañadas, S. K. Shukla, and F. Montero, "Concentration measurement of yeast suspensions using high frequency ultrasound backscattering," *Ultrasonics*, vol. 64, pp. 151–161, 2016.

[11] T. N. Hunter, J. Peakall, D. Egarr, D. M. J. Cowell, S. Freear, A. S. Tonge, L. Horton, H. P. Rice, I. Smith, K. Malone, D. Burt, M. Barnes, G. Randall, S. Biggs, and M. Fairweather, "Concentration profiling of a horizontal sedimentation tank utilising a

782   bespoke acoustic backscatter array and CFD simulations," *Chem. Eng. Sci.*, vol. 218,
783   115560, 2020.
784   [12]   P. D. Thorne and D. M. Hanes, "A review of acoustic measurement of small-scale
785   sediment processes," *Cont. Shelf Res.*, vol. 22, no. 4, pp. 603–632, Mar. 2002.
786   [13]   K. L. Deines, "Backscatter estimation using Broadband acoustic Doppler current
787   profilers," in *Proceedings of the IEEE Sixth Working Conference on Current
788   Measurement (Cat. No.99CH36331)*, 1999, pp. 249–253.
789   [14]   D. C. Fugate and C. T. Friedrichs, "Determining concentration and fall velocity of
790   estuarine particle populations using ADV, OBS and LISST," *Cont. Shelf Res.*, vol. 22,
791   no. 11–13, pp. 1867–1886, Jul. 2002.
792   [15]   A. E. Hay, "Sound scattering from a particle-laden, turbulent jet," *J. Acoust. Soc. Am.*,
793   vol. 90, no. 4, pp. 2055–2074, Oct. 1991.
794   [16]   C. M. Atkinson and H. K. Kytömaa, "Acoustic wave speed and attenuation in
795   suspensions," *Int. J. Multiph. Flow*, vol. 18, no. 4, pp. 577–592, 1992.
796   [17]   V. Stolojanu and A. Prakash, "Characterization of slurry systems by ultrasonic
797   techniques," *Chem. Eng. J.*, vol. 84, no. 3, pp. 215–222, Dec. 2001.
798   [18]   C. C. Sung, Y. J. Huang, J. S. Lai, and G. W. Hwang, "Ultrasonic measurement of
799   suspended sediment concentrations: an experimental validation of the approach using
800   kaolin suspensions and reservoir sediments under variable thermal conditions," *Hydrol.
801   Process.*, vol. 22, no. 16, pp. 3149–3154, Jul. 2008.
802   [19]   T. N. Hunter, L. Darlison, J. Peakall, and S. Biggs, "Using a multi-frequency acoustic
803   backscatter system as an in situ high concentration dispersion monitor," *Chem. Eng. Sci.*,
804   vol. 80, no. 1, pp. 409–418, Oct. 2012.
805   [20]   M. Johnson, J. Peakall, M. Fairweather, S. Biggs, D. Harbottle, and T. N. Hunter,
806   "Characterization of Multiple Hindered Settling Regimes in Aggregated Mineral
807   Suspensions," *Ind. Eng. Chem. Res.*, vol. 55, no. 37, pp. 9983–9993, 2016.
808   [21]   J. Sheng and A. E. Hay, "An examination of the spherical scatterer approximation in
809   aqueous suspensions of sand," *J. Acoust. Soc. Am.*, vol. 83, no. 2, pp. 598–610, Feb.
810   1988.
811   [22]   R. Weser, S. Wöckel, U. Hempel, B. Wessely, and J. Auge, "Particle characterization in
812   highly concentrated suspensions by ultrasound scattering method," *Sensors Actuators,
813   A Phys.*, vol. 202, pp. 30–36, 2013.
814   [23]   A. K. Hipp, G. Storti, and M. Morbidelli, "Acoustic characterization of concentrated
815   suspensions and emulsions. 2. Experimental validation," *Langmuir*, vol. 18, no. 2, pp.
816   405–412, Jan. 2002.
817   [24]   L. Schwartz and T. J. Plona, "Ultrasonic propagation in close-packed disordered
818   suspensions," *J. Appl. Phys.*, vol. 55, no. 11, pp. 3971–3977, Jun. 1984.
819   [25]   A. Shukla, A. Prakash, and S. Rohani, "Particle size monitoring in dense suspension
820   using ultrasound with an improved model accounting for low-angle scattering," *AIChE
821   J.*, vol. 56, no. 11, pp. 2825–2837, Nov. 2010.
822   [26]   X. Jia, "Codalike multiple scattering of elastic waves in dense granular media," *Phys.
823   Rev. Lett.*, vol. 93, no. 15, 154303, Oct. 2004.
824   [27]   J. H. Page, H. P. Schriemer, A. E. Bailey, and D. A. Weitz, "Experimental test of the
825   diffusion approximation for multiply scattered sound," *Phys. Rev. E*, pp. 3106–3114,
826   1995.
827   [28]   P. D. Thorne, D. Hurther, and B. D. Moate, "Acoustic inversions for measuring
828   boundary layer suspended sediment processes," *J. Acoust. Soc. Am.*, vol. 130, no. 3, pp.
829   1188–1200, Sep. 2011.
830   [29]   P. D. Thorne, P. J. Hardcastle, and R. L. Soulsby, "Analysis of acoustic measurements
831   of suspended sediments," *J. Geophys. Res.*, vol. 98, no. C1, pp. 899–910, Jan. 1993.

832   [30]   T. H. Lee and D. M. Hanes, "Direct inversion method to measure the concentration
833   profile of suspended particles using backscattered sound," *J. Geophys. Res.*, vol. 100,
834   no. C2, pp. 2649–2657, 1995.
835   [31]   G. P. Holdaway and P. D. Thorne, "Determination of a fast and stable algorithm to
836   evaluate suspended sediment parameters from high resolution acoustic backscatter
837   systems," in *Seventh International Conference on Electronic Engineering in
838   Oceanography, 1997. "Technology Transfer from Research to Industry.,"* 1997, pp. 86–
839   92.
840   [32]   E. D. Thosteson and D. M. Hanes, "A simplified method for determining sediment size
841   and concentration from multiple frequency acoustic backscatter measurements," *J.
842   Acoust. Soc. Am.*, vol. 104, no. 2, pp. 820–830, Aug. 1998.
843   [33]   D. M. Admiraal, M. H. García, and J. F. Rodríguez, "Entrainment response of bed
844   sediment to time-varying flows," *Water Resour. Res.*, vol. 36, no. 1, pp. 335–348, Jan.
845   2000.
846   [34]   D. Hurther, P. D. Thorne, M. Bricault, U. Lemmin, and J.-M. Barnoud, "A multi-
847   frequency Acoustic Concentration and Velocity Profiler (ACVP) for boundary layer
848   measurements of fine-scale flow and sediment transport processes," *Coast. Eng.*, vol.
849   58, no. 7, pp. 594–605, Jul. 2011.
850   [35]   J. Bux, J. Peakall, H. P. Rice, M. S. Manga, S. Biggs, and T. N. Hunter, "Measurement
851   and density normalisation of acoustic attenuation and backscattering constants of
852   arbitrary suspensions within the Rayleigh scattering regime," *Appl. Acoust.*, vol. 146,
853   pp. 9–22, 2019.
854   [36]   C. M. Atkinson and H. K. Kytömaa, "Acoustic properties of solid-liquid mixtures and
855   the limits of ultrasound diagnostics—I: Experiments (data bank contribution)," *J. Fluids
856   Eng.*, vol. 115, no. 4, pp. 665–675, Dec. 1993.
857   [37]   K. F. E. Betteridge, P. D. Thorne, and R. D. Cooke, "Calibrating multi-frequency
858   acoustic backscatter systems for studying near-bed suspended sediment transport
859   processes," *Cont. Shelf Res.*, vol. 28, no. 2, pp. 227–235, Feb. 2008.
860   [38]   R. J. Urick, "The absorption of sound in suspensions of irregular particles," *J. Acoust.
861   Soc. Am.*, vol. 20, no. 3, pp. 283–289, 1948.
862   [39]   M. Bricault, "Rétrodiffusion acoustique par une suspension en milieu turbulent:
863   application à la mesure de concentration pour l'étude de processus
864   hydrosédimentaires.," Grenoble Institut National Polytechnique, 2006.
865   [40]   A. Downing, P. D. Thorne, and C. E. Vincent, "Backscattering from a suspension in the
866   near field of a piston transducer," *J. Acoust. Soc. Am.*, vol. 97, no. 3, pp. 1614–1620,
867   1995.
868   [41]   K. G. Foote, "Discriminating between the nearfield and the farfield of acoustic
869   transducers," *J. Acoust. Soc. Am.*, vol. 136, no. 4, pp. 1511–1517, Oct. 2014.
870   [42]   M. A. Ainslie and J. G. McColm, "A simplified formula for viscous and chemical
871   absorption in sea water," *J. Acoust. Soc. Am.*, vol. 103, no. 3, pp. 1671–1672, 1998.
872   [43]   P. D. Thorne and M. J. Buckingham, "Measurements of scattering by suspensions of
873   irregularly shaped sand particles and comparison with a single parameter modified
874   sphere model," *J. Acoust. Soc. Am.*, vol. 116, no. 5, pp. 2876–2889, Nov. 2004.
875   [44]   I. T. MacDonald, C. E. Vincent, P. D. Thorne, and B. D. Moate, "Acoustic scattering
876   from a suspension of flocculated sediments," *J. Geophys. Res. Ocean.*, vol. 118, no. 5,
877   pp. 2581–2594, May 2013.
878   [45]   Guyson International Limited, "Blast Media Data Sheet - Guyson Honite." p. 1, 2019.
879   [46]   P. R. Smith, D. M. J. Cowell, B. Raiton, C. V. Ky, and S. Freear, "Ultrasound array
880   transmitter architecture with high timing resolution using embedded phase-locked
881   loops," *IEEE Trans. Ultrason. Ferroelectr. Freq. Control*, vol. 59, no. 1, pp. 40–49,

882   2012.

[47]   D. M. J. Cowell, S. Freear, J. Peakall, I. Smith, H. P. Rice, T. N. Hunter, D. Njobuenwu, M. Fairweather, M. Barnes, and G. Randall, "Development of a real-time acoustic backscatter system for solids concentration measurement during nuclear waste cleanup," in *2015 IEEE International Ultrasonics Symposium (IUS)*, 2015, pp. 1–4.

[48]   D. M. J. Cowell, T. Carpenter, S. Freear, J. Peakall, H. P. Rice, A. Tonge, M. Fairweather, T. N. Hunter, and M. Barnes, "Large-scale trials of a real-time acoustic backscatter system for solids concentration measurement during nuclear waste cleanup," in *IEEE International Ultrasonics Symposium, IUS*, 2016, vol. 2016-Novem.

[49]   A. Tonge, J. Bux, D. Cowell, J. Peakall, S. Freear, and T. Hunter, "Concentration profiling using a novel acoustic backscatter system with single transducers pulsed at multiple frequencies," in *IEEE International Ultrasonics Symposium, IUS*, 2017.

[50]   O. Chmiel, I. Baselt, and A. Malcherek, "Applicability of acoustic concentration measurements in suspensions of artificial and natural sediments using an acoustic doppler velocimeter," *Acoustics*, vol. 1, no. 1. pp. 59–77, 2018.

[51]   M. Salehi and K. Strom, "Using velocimeter signal to noise ratio as a surrogate measure of suspended mud concentration," *Cont. Shelf Res.*, vol. 31, no. 9, pp. 1020–1032, Jun. 2011.

[52]   V. Twersky, "Acoustic bulk parameters in distributions of pair-correlated scatterers," *J. Acoust. Soc. Am.*, vol. 64, no. 6, pp. 1710–1719, Dec. 1978.

[53]   A. Tourin, M. Fink, and A. Derode, "Multiple scattering of sound," *Waves in Random Media*, vol. 10, no. 4, pp. R31–R60, Oct. 2000.

[54]   J. Carlson and P.-E. Martinsson, "A simple scattering model for measuring particle mass fractions in multiphase flows," *Ultrasonics*, vol. 39, no. 8, pp. 585–590, Jun. 2002.

[55]   T. N. Hunter, S. P. Usher, S. Biggs, P. J. Scales, A. D. Stickland, and G. V. Franks, "Characterization of bed densification in a laboratory scale thickener, by novel application of an acoustic backscatter system," *Procedia Eng.*, vol. 102, pp. 858–866, Jan. 2015.

[56]   A. S. Dukhin and P. J. Goetz, "New developments in acoustic and electroacoustic spectroscopy for characterizing concentrated dispersions," *Colloids Surfaces A Physicochem. Eng. Asp.*, vol. 192, no. 1–3, pp. 267–306, Nov. 2001.

[57]   R. E. Challis, M. J. W. Povey, M. L. Mather, and A. K. Holmes, "Ultrasound techniques for characterizing colloidal dispersions," *Reports Prog. Phys.*, vol. 68, no. 7, pp. 1541–1637, 2005.

[58]   M. Tourbin and C. Frances, "A survey of complementary methods for the characterization of dense colloidal silica," *Part. Part. Syst. Charact.*, vol. 24, no. 6, pp. 411–423, Dec. 2007.

[59]   P. D. Thorne and R. Meral, "Formulations for the scattering properties of suspended sandy sediments for use in the application of acoustics to sediment transport processes," *Cont. Shelf Res.*, vol. 28, no. 2, pp. 309–317, Feb. 2008.

[60]   P. D. Thorne and D. Hurther, "An overview on the use of backscattered sound for measuring suspended particle size and concentration profiles in non-cohesive inorganic sediment transport studies," *Cont. Shelf Res.*, vol. 73, pp. 97–118, Feb. 2014.

[61]   A. L. Bowler, S. Bakalis, and N. J. Watson, "A review of in-line and on-line measurement techniques to monitor industrial mixing processes," *Chem. Eng. Res. Des.*, vol. 153, pp. 463–495, 2020.